minerals

MDPI

Article

Zircon LA-ICP-MS U-Pb Ages and the Hf Isotopic Composition of the Ore-Bearing Porphyry from the Yanghuidongzi Copper Deposit, Heilongjiang, China, and Its Geological Significance

Diange Cong [1,2], Hongli Pang [3,*], Shuzhi Wang [4], Ying Tian [5], Hui Ying [6] and Guobiao Huang [7]

1. Department of Geological Engineering, Qinghai University, Xining 810016, China; congdiange@163.com
2. Qinghai Geological Survey Institute, Xining 810012, China
3. School of Economic & Managment, Shanghai Maritime University, Shanghai 201306, China
4. North China University of Science and Technology, Tangshan 063210, China; wangszh1987@163.com
5. Hebei Provincial Institute of Geology and Mineral Resources Research, Langfang 065000, China; tianying1001@163.com
6. Qinghai Fifth Geological Exploration Institute, Xining 810028, China; yinghui9102@163.com
7. Qaidam Comprehensive Geology and Mineral Exploration Institute of Qinghai Province, Golmud 816000, China; huangguobiao2019@163.com

* Correspondence: Panghl12@lzu.edu.cn; Tel.: +021-38282425

Received: 26 September 2019; Accepted: 30 October 2019; Published: 2 November 2019

Abstract: The Yanghuidongzi copper deposit is a typical porphyry copper deposit located at the eastern margin of the Xing'anling-Mongolian Orogenic Belt (XMOB). While much attention have been paid to the ore-forming age of the deposit and the magma source of the ore-bearing porphyry, this paper approaches this issue with the methods of the LA-ICP-MS zircon U-Pb dating and Lu-Hf isotopic composition of the Yanghuidongzi porphyry copper deposit. The results reveal that the Yanghuidongzi porphyry copper deposit was formed in the Early Jurassic (189.6 ± 1.0 Ma), which corresponds to the time of magmatic activity in this region. The background studies of ore-forming dynamics indicate that the formation of the Yanghuidongzi copper deposit is related to the subduction of the Paleo-Pacific plate. The Yanghuidongzi ore-bearing porphyry zircons have a positive $\varepsilon_{\mathrm{Hf}}(t)$ value (4.4–7.0), a high ^{176}Hf/^{177}Hf ratio (0.282786–0.282854), and a two-stage Hf model ages (T_{DM2}) ranging from 783 Ma to 943 Ma, all of which suggest that the Early Jurassic granodiorite porphyry of the Yanghuidongzi deposit was formed by the partial melting of newly grown crustal material from the depleted mantle in the Neoproterozoic.

Keywords: zircon U-Pb ages; Hf isotopic composition; porphyry copper deposit; Yanghuidongzi deposit

1. Introduction

Porphyry deposits are mainly formed at the boundary of converging plates, including island arcs [1–5], continental margin arcs [4,6–8], and continental collision environments [9–13]. Thus, porphyry deposits are important geological markers for discussing regional tectonic evolution and tectonic settings [14]. The U-Pb isotopic system in natural zircon has a closure temperature greater than 900 °C [15,16], so zircons are regarded as ideal minerals for determining the age of magma crystallization [17]. Furthermore, zircons have a high Hf concentration (0.5–2%) and can maintain their original Hf isotopic composition even in the case of granulite facies, which could record the information of the magma source and magmatic activity [18–20].

The Yanghuidongzi copper deposit is located at the eastern margin of the Xing'anling-Mongolian Orogenic Belt (XMOB), which has great economic value. Previous studies have been carried out on the wall rock alteration characteristics, geochemical characteristics, the source of ore-forming elements, the migration and evolution of ore-forming fluids, and the mineralization of the deposit [21,22]. All evidence shows that the deposit is a typical porphyry deposit [22]. However, the ore-forming age of the deposit and the magma source of the ore-bearing porphyry are still issues of concern.

Based on a study of zircon geochronology and the Hf isotopic composition of the ore-bearing porphyry in the Yanghuidongzi copper deposit, the ore-forming age, metallogenic dynamics background, and magma source are discussed. The research results also help us understand the geological evolution history of the eastern XMOB and the genesis of the porphyry copper deposits in the area.

2. Geological Setting

2.1. Regional Geology

The Yanghuidongzi copper deposit is located in the Jiamusi–Xingkai block at the eastern margin of the XMOB, adjacent to the Russian border in the east and the Dunhua–Mishan fault to the west (Figure 1a,b). The study area belongs to the Paleo-Asian tectonic domain and the Pacific Ocean tectonic domain complex.

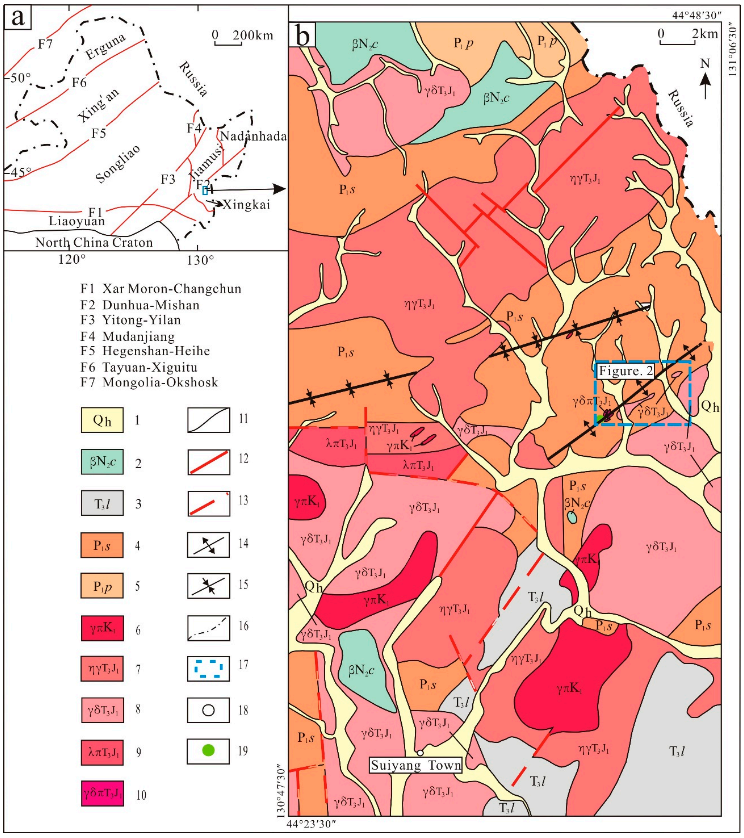

Figure 1. (**a**) The structural location map of the Yanghuidongzi mining area [23] and (**b**) regional geological map of the Yanghuidongzi area [24,25]: 1—Holocene; 2—the Neogene Chuandishan basalt Formation; 3—the Triassic Luoquanzhan Formation; 4—the lower Permian Shuangqiaozi Formation; 5—the lower Permian Pingyangzhen Formation; 6—Early Cretaceous granite porphyry; 7—Late Triassic-Early Jurassic monzonitic granite; 8—Late Triassic-Early Jurassic granodiorite; 9—Late Triassic–Early Jurassic rhyolite porphyry; 10—Late Triassic–Early Jurassic granodiorite porphyry; 11—Geological boundary; 12—measured fault; 13—inferred fault; 14—anticline; 15—syncline; 16—national border line; 17—Yanghuidongzi mining area; 18—residence point; 19—copper deposit.

The strata in the area primarily comprise the lower Permian Pingyangzhen Formation (P_1p), the lower Permian Shuangqiaozi Formation (P_1s), the Triassic Luoquanzhan Formation (T_3l), the Neogene Chuandishan Formation (βN_2c), and the Holocene (Qh) (Figure 1b). The magmatism in the area is intense, and intermediate-acid intrusive rocks of the Middle-Late Triassic, Early Jurassic, and Early Cretaceous are widely developed (Figure 1b). The Dunhua–Mishan deep fault (F2) of the Mesozoic is closely related to the magmatism, and the NW–NE trending faults have established the structure pattern of the study area (Figure 1b).

2.2. Deposit Geology

The Lower Permian Shuangqiaozi Formation (P_1s) is widely exposed in the mining area (Figure 2a). This unit consists of a set of low-grade metamorphic rocks, including carbonaceous sericite phyllite, biotite quartz schist, and albite feldspar schist. The carbonaceous sericite phyllite are characterized by fine-grained granular crystalloblastic texture and phyllitic structure, mainly consist of quartz and sericite, with a small amount of biotite, chlorite, garnet, feldspar and opaque minerals. The biotite quartz schists are distributed in district 2 and district 3, have granular crystalloblastic structure, laminated crystalloblastic texture and schistose structure. The dominate mineral is quartz, and the secondary minerals are biotite, sericite, plagioclase and chlorite. The albite feldspar schists are distributed in district 2 and interbedded with biotite quartz schists, which are mainly composed of actinolite, and following are albite, calcite, biotite, and quartz, with fine-grained columnar crystalloblastic texture and schistose structure. Folds and faults in the mining area are relatively developed. The Yanwangdian anticline runs through the whole area, with an axial strike of NE 55°, dipping to NW and SE (Figure 1b). During the structural extrusion process, the fracture zone generated in the anticline shaft provides a good enrichment site for ore filling. The faults are divided into two stages: pre-mineralization and post-mineralization. The pre-mineralization faults are SN trending (F1, F2, F3) and oblique to the anticline of the Yanwangdian anticline. Their intersection controls the location of the ore-bearing rock mass. The post-mineralization faults are NW and NWW trending (F4–F8), which causes the rock mass to become misaligned.

The intrusive rocks in the mining area are dominated by granodiorite ($\gamma\delta T_3J_1$), granodiorite porphyry ($\gamma\delta\pi T_3J_1$), and mica–plagioclase lamprophyre ($\chi\xi\chi$). The granodiorite is mostly distributed in district 2 and district 3 (Figure 2a), while the granodiorite porphyry closely related to the mineralization is distributed only in district 1 (Figure 2a). The ore-bearing porphyry carried a large number of volatile components during the intrusion process, and great pressure was formed at the contact zone between the magma and the surrounding rock, and the surrounding rock of the contact zone was strongly broken to form breccia. Then, the breccia was filled and cemented by the ore-bearing hydrothermal fluid [21]. The breccia is mainly composed of sericite phyllite, granodiorite porphyry, and quartz vein and is mainly distributed in the contact between the granodiorite porphyry and surrounding rocks (Figure 2b).

There are 13 ore bodies in the Yanghuidongzi deposit, of which the six ones (II, VIII, X, XI, XII, XIII) distributed in district 1 display an industrial development potential (Figure 2b,c). The spatial position of the six economic ore bodies is controlled by the NE-trending structure. The morphology of the ore bodies is restricted by the four veined granodiorite porphyry bodies and the tectonic fracture zone among the surrounding rocks. The metal minerals in the ore are mainly chalcopyrite, pyrite, and sphalerite. The wall rock alteration of the deposit is characterized by the silicization zone (H1), the biotite-quartz-sericitization zone (H2), the quartz-sericitization (muscovitization) zone (H3), and the propylitization zone (H4), with typical porphyry copper deposit alteration zoning. The H2 and H3 zones are the main locations of economic ore bodies (Figure 2a,b).

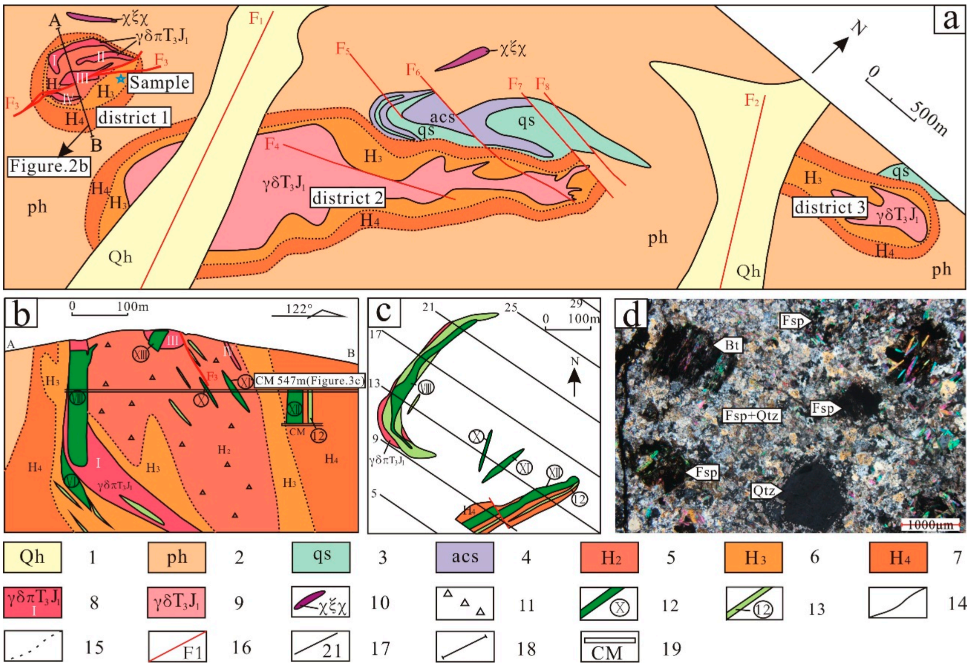

Figure 2. (**a**) Geological map of the Yanghuidongzi deposit [24], (**b**) profile of exploration Line 13 (A–B) [24], (**c**) the tunnel engineering plan at a 547 m elevation in the Yanghuidongzi deposit [24], (**d**) a photomicrograph of the YHD3 samples: 1—Holocene series, 2—carbonaceous sericite phyllite, 3—biotite quartz schist, 4—sodium feldspar shale schist, 5—biotite-quartz-sericitization (muscovitization) zone (H2), 6—quartz-sericitization (muscovitization) zone (H3), 7—propylitization zone (H4), 8—Late Triassic-Early Jurassic granodiorite porphyry and number, 9—Late Triassic-Early Jurassic granodiorite, 10—mica-plagioclase lamprophyre, 11—breccia, 12—copper ore body and number, 13—copper mineralization and number, 14—geological boundary, 15—alteration boundary, 16—fault and number, 17—exploration line and number, 18—section line and number, 19—tunnel engineering plan and number Qtz—quartz, Bt—biotite, Fsp—Feldspar.

3. Sample Collection and Analysis Methods

It was not possible to collect fresh rock samples in the field, as the shallow porphyry in the Yanghuidongzi copper deposit experienced varying degrees of hydrothermal alteration. The sample analyzed in this paper is the ore-bearing granodiorite porphyry (YHD3) from the altered zone H3 (Figure 2a). The rock underwent a certain degree of hydrothermal alteration and has a massive structure, metamorphic texture, residual plaque-matrix crystallite texture, and euhedral-granular texture (Figure 2d). The rock is composed of phenocrysts and a matrix. The phenocrysts are composed of quartz, feldspar pseudomorph, and biotite pseudomorph, with particle sizes ranging from 0.5 mm to 1.0 mm. The original euhedral platy feldspar is decomposed into sericite, muscovite, and quartz, among others. The altered minerals are fine in size, appearing in the form of aggregates. The original leafy biotite appears to be an illusion after being replaced by muscovite, carbonate, quartz, and limonite. The original leaf-like biotites appear as pseudomorph after being replaced by muscovite, carbonate, quartz and limonite. The matrix consists mainly of feldspar and quartz, which develop muscovitization, sericitization, quartzization, carbonation, and limonitization. Although the rock has undergone a certain degree of alteration, its granitic texture and the crystal form of its original minerals are still substantially retained.

Zircon sorting was carried out in the laboratory of the Regional Geological Survey Institute of Hebei Province (Langfang, China). Almost 500 kg of the sample was crushed, panned, electromagnetically selected, and subjected to heavy liquid separation. Zircons with no obvious cracks, less inclusions, and intact crystal forms were selected under a binocular microscope. The target zircon cathodoluminescence (CL) image and zircon U-Pb dating were carried out at the Key Laboratory of Mineral Resources

Evaluation in Northeast Asia, Ministry of Land and Resources, Jilin University, Changchun, China. Helium was used as a carrier gas to provide efficient aerosol to the ICP and minimize aerosol deposition around the ablation site and in the transport tube [26,27]. Argon was used as the supplementary gas and mixed with the carrier gas via a T-connector before entering the ICP. A spot size of 32 μm and a 7 Hz repetition rate were used for the analyses. The standard zircon 91500 [28] was used as an external standard for the U-Pb analyses. Isotopic rations were calculated using the GLITTER program (version 4.0, GEOMOC National Laboratory, Sydney, New South Wales, Australia) with a common Pb correction, following the method of Yuan et al. [29]. Uncertainties of the isotope ratios were assigned with a 1σ error, and weighted mean ages were calculated at a 1σ confidence level. The age calculation and concordia diagram plotting were processed using the ISOPLOT program (Version 3.0, Berkeley Geochronology Center, Berkeley, CA, USA) [30].

The zircon Lu-Hf isotopic composition analyses were carried out at Nanjing FocuMS Technology Co. Ltd. (Nanjing, China) with a *RESOlution LR* 193 nm ArF excimer laser (Australian Scientific Instruments, Canberra, Australia) and a *Nu Plasma II* MC-ICP-MS (Nu Instruments, Wrexham, Wales, UK). During the experiment, helium was used as the carrier gas for the ablation material, and the laser beam's spot diameter was 50 μm. The internationally accepted standard zircon (91500) was used as the reference material in this test [31]. Detailed analytical procedures are described in Wu et al. [32]. The $^{176}Hf/^{177}Hf$ value of the standard zircon (91500) tested in this experiment was 0.2822906 ± 12 (1δ), which is consistent with the value of the predecessor [33] within the error range. In the calculation of the $\varepsilon Hf(t)$ values, the $^{176}Hf/^{177}Hf$ and $^{176}Lu/^{177}Hf$ ratios of present-day chondrite and the depleted mantle were (0.0332, 0.282772) and (0.0384, 0.28325), respectively [34,35]. The two-stage Hf model ages (T_{DM2}) were calculated by adopting $^{176}Lu/^{177}Hf$ = 0.015 for the average continental crust [36].

4. Results

4.1. Zircon Morphology

Zircon CL images with their numbers are shown in Figure 3. The zircon grains (YHD3) are colorless and euhedral prismatic, with lengths of about 100–230 μm and aspect ratios of about 2–4.5. All zircons have strong CL and develop oscillatory zoning. The rims of the zircons are finely oscillatory zoned, while their cores are faint and broadly zoned, similar to typical the features of magmatic zircons [17,37].

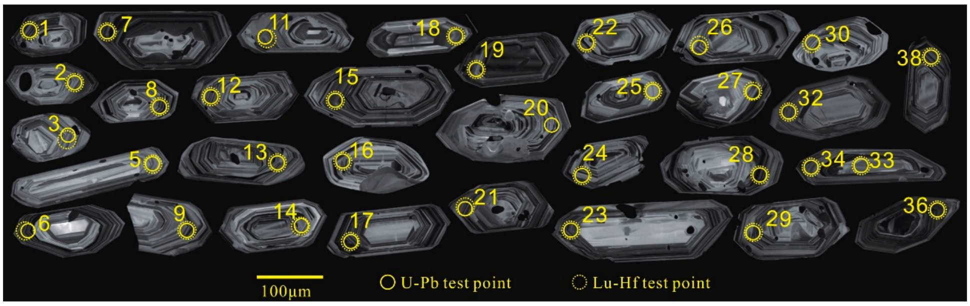

Figure 3. Zircon Cathodoluminescence (CL) images of the Yanghuidongzi porphyry. The 1–38 represents laser ablation spot number.

4.2. Zircon U-Pb Age

In this paper, a total of 38 points were analyzed (Table 1). The content of Th in the zircons ranged from 33.43 ppm to 259.75 ppm, and the content of U ranged from 61.14 ppm to 815.29 ppm. The Th/U ratios of the zircons were all greater than 0.1 (0.11–0.68), indicating that most of the zircons had an igneous origin. On the basis of the zircon U-Pb isotope analysis, we found that 33 points had a good concordant relationship. The $^{206}Pb/^{238}U$ values from the 33 points are listed in Table 1, which shows that the zircon's U-Pb age is 189.6 ± 1.0 Ma (MSWD = 0.93, n = 33) (Figure 4).

Table 1. Zircon LA-ICP-MS U-Pb analysis of granodiorite porphyries in the Yanghuidongzi deposit.

Spot No.	Th (ppm)	U (ppm)	Th/U	U-Th-Pb Isotope Ratio and Error								Age/Ma and Error	
				$^{207}Pb/^{206}Pb$	1σ	$^{207}Pb/^{235}U$	1σ	$^{206}Pb/^{238}U$	1σ	$^{208}Pb/^{232}Th$	1σ	$^{206}Pb/^{238}U$	1σ
YHD-3-01	112.77	277.75	0.41	0.04866	0.0018	0.20314	0.0072	0.03028	0.0005	0.00935	0.0002	192	3
YHD-3-02	66.97	186.41	0.36	0.05199	0.0026	0.2052	0.0099	0.02863	0.0005	0.00882	0.0003	182	3
YHD-3-03	71.07	158.93	0.45	0.05054	0.002	0.20974	0.0082	0.0301	0.0005	0.00961	0.0003	191	3
YHD-3-05	43.90	131.68	0.33	0.0493	0.0041	0.20712	0.0169	0.03047	0.0008	0.01077	0.0007	193	5
YHD-3-06	77.89	162.05	0.48	0.05144	0.0025	0.21036	0.0098	0.02966	0.0005	0.01046	0.0004	188	3
YHD-3-07	81.76	583.62	0.14	0.05037	0.0011	0.20902	0.0047	0.0301	0.0004	0.00978	0.0003	191	2
YHD-3-08	91.49	278.36	0.33	0.0497	0.0015	0.20649	0.0063	0.03013	0.0004	0.00937	0.0002	191	3
YHD-3-09	90.68	318.84	0.28	0.05207	0.0018	0.21261	0.0073	0.02961	0.0004	0.01046	0.0003	188	3
YHD-3-11	51.23	215.60	0.24	0.05611	0.0019	0.22979	0.0078	0.0297	0.0005	0.00946	0.0003	189	3
YHD-3-12	67.73	163.68	0.41	0.05039	0.002	0.21345	0.0083	0.03072	0.0005	0.00925	0.0003	195	3
YHD-3-13	138.81	336.32	0.41	0.05127	0.0016	0.2072	0.0064	0.02931	0.0004	0.00863	0.0002	186	3
YHD-3-14	60.18	187.12	0.32	0.05131	0.0026	0.21053	0.0105	0.02976	0.0005	0.0099	0.0004	189	3
YHD-3-15	128.81	362.03	0.36	0.04924	0.0014	0.20463	0.0056	0.03014	0.0004	0.00968	0.0002	191	3
YHD-3-16	108.03	221.36	0.49	0.05082	0.0018	0.21009	0.0075	0.02998	0.0005	0.00981	0.0003	190	3
YHD-3-17	156.22	439.30	0.36	0.05179	0.0013	0.2153	0.0054	0.03015	0.0004	0.01009	0.0002	191	3
YHD-3-18	126.09	211.00	0.60	0.05004	0.0023	0.20327	0.0092	0.02946	0.0005	0.00955	0.0003	187	3
YHD-3-19	59.67	306.46	0.19	0.0507	0.0015	0.20876	0.0061	0.02986	0.0004	0.01017	0.0003	190	3
YHD-3-20	70.13	192.51	0.36	0.05038	0.0022	0.20924	0.0091	0.03012	0.0005	0.01025	0.0004	191	3
YHD-3-21	45.73	234.19	0.20	0.04972	0.0017	0.20585	0.0069	0.03003	0.0004	0.00959	0.0003	191	3
YHD-3-22	60.16	159.37	0.38	0.05289	0.0021	0.21777	0.0083	0.02986	0.0005	0.01099	0.0003	190	3
YHD-3-23	70.51	150.73	0.47	0.04866	0.002	0.20268	0.008	0.03021	0.0005	0.00916	0.0003	192	3
YHD-3-24	115.09	273.36	0.42	0.05043	0.0018	0.20809	0.0073	0.02992	0.0005	0.00933	0.0003	190	3
YHD-3-25	128.35	188.49	0.68	0.05224	0.0032	0.21021	0.0124	0.02918	0.0006	0.00923	0.0003	185	4
YHD-3-26	106.94	200.01	0.53	0.05136	0.002	0.21126	0.0081	0.02983	0.0005	0.00896	0.0003	189	3
YHD-3-27	34.15	85.33	0.40	0.05047	0.0028	0.20344	0.0109	0.02923	0.0005	0.0084	0.0004	186	3
YHD-3-28	102.94	392.42	0.26	0.05562	0.0018	0.23039	0.0071	0.03004	0.0004	0.01085	0.0003	191	3
YHD-3-29	94.86	241.10	0.39	0.05122	0.0018	0.21241	0.0073	0.03008	0.0005	0.00977	0.0003	191	3
YHD-3-30	33.43	117.48	0.28	0.05018	0.0026	0.20831	0.0106	0.03011	0.0005	0.01063	0.0005	191	3
YHD-3-32	58.98	190.17	0.31	0.05031	0.0018	0.21086	0.0072	0.03039	0.0005	0.00941	0.0003	193	3
YHD-3-33	36.83	61.14	0.60	0.05048	0.0045	0.20796	0.018	0.02988	0.0008	0.01022	0.0006	190	5
YHD-3-34	123.07	382.65	0.32	0.05287	0.0026	0.20779	0.0098	0.02851	0.0005	0.00889	0.0004	181	3
YHD-3-36	37.92	333.64	0.11	0.05109	0.0015	0.21124	0.0061	0.02999	0.0004	0.0101	0.0004	190	3
YHD-3-38	127.17	298.07	0.43	0.05053	0.0016	0.21012	0.0064	0.03016	0.0004	0.00993	0.0002	192	3

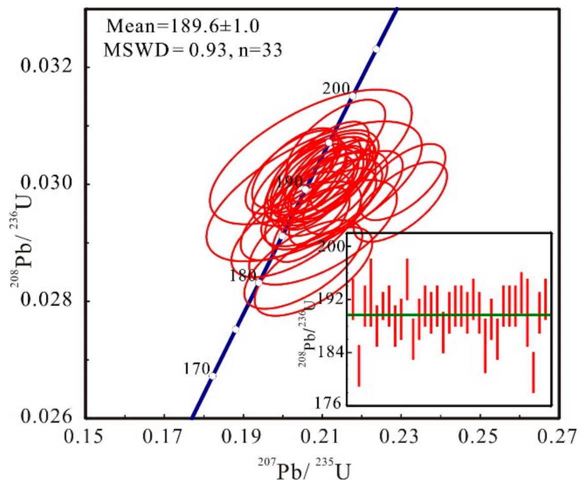

Figure 4. Zircon U-Pb age concordia diagram.

4.3. Zircon Trace Element Characteristics

The trace element analysis results of the ore-bearing porphyry (YHD3) zircons are shown in Table 2. The range of ∑REE was 328.79–1195.81 ppm (mean = 1195.81 ppm), ∑LREE is 3.22–229.94 ppm (mean = 37.37 ppm), ∑HREE was 319.61–1179.99 ppm (mean = 527.76 ppm), and $(La/Sm)_N$ was 0.85–4414.71 ppm (mean = 267.89 ppm). The chondrite-normalized REE patterns (Figure 5a) show that the zircons were enriched in HREE and depleted in LREE, with a δCe positive anomaly (1.07–86.94, mean = 18.18) and a δEu negative anomaly (0.06–0.47, mean = 0.16).

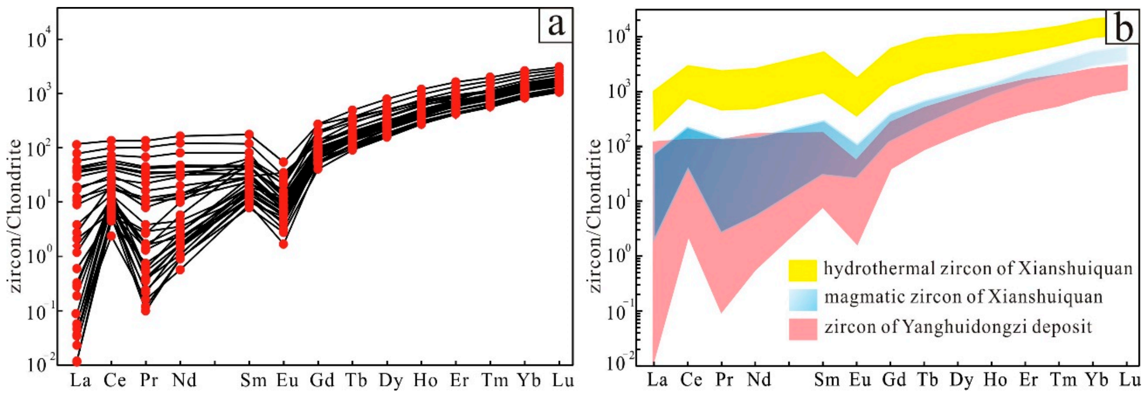

Figure 5. (**a**) Yanghuidongzi zircons chondrite-normalized REE patterns, (**b**) a comparison of zircon chondrite-normalized REE patterns in Yanghuidongzi and Xianshuiquan (the Xianshuiquan values are from Tang et al. [38]; normalization values are from McDonough and Sun (1995) [39]).

Table 2. Analysis of rare earth elements in zircons (ppm).

Spot No.	La	Ce	Pr	Nd	Sm	Eu	Gd	Tb	Dy	Ho	Er	Tm	Yb	Lu	ΣREE	LREE	HREE	δEu	δCe	$(Sm/La)_N$
YHD-3-01	0.02	9.71	0.06	1.32	3.47	0.61	23.22	8.40	95.85	35.46	123.71	31.01	295.73	55.91	684.47	15.18	669.29	0.16	47.09	262.20
YHD-3-02	0.37	5.76	0.15	1.06	1.52	0.31	10.42	3.67	41.98	15.56	67.57	14.24	138.92	27.25	328.79	9.18	319.61	0.17	5.89	6.35
YHD-3-03	0.91	8.39	0.37	2.10	2.53	0.42	13.81	4.96	54.77	19.80	82.78	16.64	159.42	30.43	397.33	14.72	382.61	0.17	3.57	4.30
YHD-3-05	0.07	5.10	0.04	0.75	1.80	0.26	11.37	4.03	45.38	16.67	72.47	15.22	150.11	29.06	352.32	8.01	344.31	0.13	23.83	39.67
YHD-3-06	4.47	16.57	2.09	13.76	9.62	1.49	41.56	12.67	128.07	41.48	156.10	28.88	248.73	43.67	749.16	48.00	701.16	0.19	1.32	3.33
YHD-3-07	0.50	3.99	0.27	1.66	1.96	0.23	13.39	5.24	65.41	24.87	113.56	25.00	251.38	48.92	556.38	8.61	547.77	0.10	2.62	6.09
YHD-3-08	0.01	6.07	0.04	0.50	2.46	0.31	14.84	5.50	63.76	22.87	96.25	19.84	188.80	35.66	456.91	9.39	447.52	0.12	47.10	448.30
YHD-3-09	13.57	44.67	6.40	37.68	12.38	0.75	21.61	5.75	58.00	20.04	84.74	17.09	164.76	31.47	518.91	115.45	403.46	0.14	1.17	1.41
YHD-3-11	2.11	10.75	1.00	5.37	3.62	0.43	15.51	5.29	59.91	21.99	95.71	20.51	199.38	38.91	480.49	23.28	457.21	0.15	1.81	2.66
YHD-3-12	0.08	5.75	0.06	1.05	2.36	0.35	11.53	4.26	47.58	17.56	72.88	14.70	142.37	27.44	347.97	9.65	338.32	0.17	19.63	47.23
YHD-3-13	0.01	7.10	0.03	0.79	2.59	0.40	17.30	6.30	72.95	26.77	115.26	23.93	228.09	43.68	545.20	10.92	534.28	0.14	57.12	303.94
YHD-3-14	6.96	24.38	2.68	14.90	5.14	0.52	16.41	5.89	66.57	24.90	110.39	23.00	221.71	44.09	567.54	54.58	512.96	0.16	1.38	1.14
YHD-3-15	0.04	6.30	0.05	0.77	2.13	0.33	15.65	5.69	65.47	23.72	103.08	21.79	209.48	40.06	494.56	9.62	484.94	0.12	28.67	73.71
YHD-3-16	10.34	36.21	4.25	22.33	7.19	0.73	20.74	6.37	69.92	24.82	101.67	20.42	194.77	37.17	556.93	81.05	475.88	0.17	1.34	1.08
YHD-3-17	0.07	7.00	0.12	1.28	4.28	0.49	27.79	10.61	119.60	43.46	182.70	37.56	341.65	62.66	839.27	13.24	826.03	0.10	14.48	100.60
YHD-3-18	0.00	3.77	0.14	2.68	7.98	1.25	55.82	18.27	200.12	67.25	268.42	50.49	441.62	78.00	1195.81	15.82	1179.99	0.13	8.59	4414.71
YHD-3-19	0.01	3.30	0.01	0.42	1.79	0.18	12.82	4.93	63.84	24.00	109.12	23.72	234.16	45.28	523.58	5.71	517.87	0.09	81.01	341.36
YHD-3-20	-	4.39	0.02	0.68	1.80	0.25	10.96	4.04	46.34	16.62	73.20	14.91	144.14	27.94	345.28	7.13	338.15	0.13	65.84	0.00
YHD-3-21	0.01	3.17	0.02	0.44	1.21	0.16	8.31	3.38	39.57	15.25	70.22	15.31	150.10	29.34	336.49	5.01	331.48	0.11	39.05	339.94
YHD-3-22	8.93	28.26	3.36	16.96	4.91	0.39	13.36	3.88	46.00	16.72	71.42	14.99	143.90	28.18	401.26	62.81	338.45	0.14	1.26	0.85
YHD-3-23	0.14	3.32	0.25	4.64	9.13	1.22	38.01	11.13	112.92	37.10	146.19	26.94	247.25	44.89	683.13	18.70	664.43	0.17	3.35	100.59
YHD-3-24	0.28	7.18	0.16	1.56	2.87	0.39	17.92	6.70	78.11	28.77	121.33	24.45	234.54	44.57	568.84	12.45	556.39	0.13	8.11	15.88
YHD-3-25	8.35	27.19	3.15	16.63	6.33	0.93	23.79	7.43	80.38	27.38	110.09	21.47	195.43	35.84	564.39	62.58	501.81	0.20	1.30	1.17
YHD-3-26	4.02	18.90	1.54	9.34	4.44	0.52	19.00	6.18	68.19	23.79	101.43	19.98	187.36	35.57	500.25	38.75	461.50	0.15	1.86	1.71
YHD-3-27	0.01	2.76	0.07	0.92	2.87	0.72	18.42	6.44	74.98	27.37	114.25	22.52	212.21	40.22	523.75	7.34	516.41	0.23	11.92	1646.55
YHD-3-28	18.55	61.08	9.70	57.06	18.16	1.75	29.00	7.43	71.89	24.20	99.59	20.59	189.43	34.87	643.30	166.30	477.00	0.23	1.11	1.52
YHD-3-29	9.79	32.32	3.94	20.84	6.76	0.61	18.88	6.33	69.91	24.42	105.96	20.90	208.09	38.57	567.32	74.26	493.06	0.15	1.28	1.07
YHD-3-30	2.86	11.18	1.14	6.75	4.23	0.48	16.83	5.62	62.14	21.73	94.92	19.41	186.58	36.41	470.28	26.64	443.64	0.15	1.52	2.29
YHD-3-32	0.01	4.68	0.01	0.42	1.67	0.26	10.59	3.61	42.77	15.93	69.68	14.51	140.07	26.83	331.04	7.05	323.99	0.14	86.94	191.05
YHD-3-33	27.82	82.62	12.80	76.55	27.00	3.15	55.18	13.78	128.30	39.80	152.20	28.27	256.23	47.35	951.05	229.94	721.11	0.24	1.07	1.50
YHD-3-34	2.55	14.14	0.96	6.58	6.74	0.81	38.40	13.63	156.47	54.09	221.70	43.36	394.44	69.57	1023.44	31.78	991.66	0.12	2.21	4.10
YHD-3-36	0.01	1.45	0.02	0.27	1.39	0.10	10.17	4.27	54.88	21.03	97.49	21.72	217.95	41.77	472.50	3.22	469.28	0.06	22.69	195.46
YHD-3-38	0.65	12.72	0.75	6.05	4.55	2.02	24.60	8.61	92.84	33.20	139.20	28.32	268.31	49.52	671.34	26.74	644.60	0.47	3.89	10.83

4.4. Zircons Hf Isotopic Composition

Based on the LA-ICP-MS zircon U-Pb data, we analyzed the zircon Lu-Hf isotope on the same spots of the concordant grains (YHD3). The results of the Hf isotope are shown in Table 3. The $^{176}Lu/^{177}Hf$ ratios of the Yanghuidongzi zircons were lower (0.000443–0.001193, average value = 0.000654). The ^{176}Hf generated by ^{176}Lu is very rare, which indicates that most of the zircons have little accumulation of radioactive Hf after the zircons formation. Because of the lower $^{176}Hf/^{177}Hf$ ratios in the zircons, we assume that the measured values of $^{176}Hf/^{177}Hf$ are equivalent to the initial $^{176}Hf/^{177}Hf$ ratios of the zircon [20]. Furthermore, the $\varepsilon_{Hf}(t)$ value of the Yanghuidongzi zircons was 4.4–7.0 (mean = 5.8), the $^{176}Hf/^{177}Hf$ value was 0.282786–0.282854 (mean = 0.282820), and the two-stage Hf model ages (T_{DM2}) ranged from 783 Ma to 943 Ma (mean = 861 Ma).

Table 3. The results of the Hf isoptope analysis for the single-grain zircon in the ore-bearing porphyry of the Yanghuidongzi deposit.

Spot No.	Age (Ma)	$^{176}Yb/^{177}Hf$	$^{176}Lu/^{177}Hf$	$^{176}Hf/^{177}Hf$	1σ	$\varepsilon_{Hf}(t)$	T_{DM1}(Ma)	T_{DM2}(Ma)	$f_{Lu/Hf}$
YHD-3-01	192	0.016771	0.000627	0.282800	0.000014	5.1	634	904	−0.98
YHD-3-02	182	0.014267	0.000537	0.282812	0.000012	5.4	616	882	−0.98
YHD-3-03	191	0.017620	0.000651	0.282830	0.000011	6.2	593	838	−0.98
YHD-3-05	193	0.015195	0.000565	0.282823	0.000011	6.0	601	851	−0.98
YHD-3-06	188	0.024575	0.000811	0.282816	0.000011	5.6	614	871	−0.98
YHD-3-07	191	0.015804	0.000574	0.282816	0.000010	5.7	611	868	−0.98
YHD-3-08	191	0.016230	0.000598	0.282798	0.000011	5.0	637	910	−0.98
YHD-3-09	188	0.014137	0.000519	0.282827	0.000009	6.0	595	846	−0.98
YHD-3-11	189	0.014716	0.000548	0.282818	0.000010	5.7	608	866	−0.98
YHD-3-12	195	0.012191	0.000443	0.282842	0.000011	6.7	573	807	−0.99
YHD-3-13	186	0.018696	0.000710	0.282802	0.000015	5.1	633	904	−0.98
YHD-3-14	189	0.018856	0.000697	0.282803	0.000012	5.2	631	899	−0.98
YHD-3-15	191	0.017175	0.000628	0.282808	0.000011	5.4	623	886	−0.98
YHD-3-16	190	0.020347	0.000736	0.282815	0.000014	5.6	615	873	−0.98
YHD-3-17	191	0.021627	0.000748	0.282837	0.000011	6.4	584	822	−0.98
YHD-3-18	187	0.034464	0.001193	0.282842	0.000013	6.4	585	818	−0.96
YHD-3-19	190	0.013862	0.000504	0.282845	0.000010	6.7	569	803	−0.98
YHD-3-20	191	0.015326	0.000557	0.282792	0.000012	4.8	644	922	−0.98
YHD-3-21	191	0.012012	0.000448	0.282794	0.000012	4.9	640	918	−0.99
YHD-3-22	190	0.020834	0.000754	0.282829	0.000011	6.1	596	842	−0.98
YHD-3-23	192	0.019914	0.000677	0.282829	0.000013	6.1	595	840	−0.98
YHD-3-24	190	0.012887	0.000478	0.282838	0.000012	6.4	579	819	−0.99
YHD-3-25	185	0.020151	0.000723	0.282837	0.000015	6.3	585	827	−0.98
YHD-3-26	189	0.019277	0.000689	0.282828	0.000012	6.0	596	843	−0.98
YHD-3-27	186	0.021796	0.000791	0.282788	0.000016	4.5	655	937	−0.98
YHD-3-28	191	0.013182	0.000472	0.282837	0.000013	6.5	580	819	−0.99
YHD-3-29	191	0.013565	0.000498	0.282854	0.000013	7.0	557	783	−0.99
YHD-3-30	191	0.018706	0.000691	0.282819	0.000013	5.8	609	863	−0.98
YHD-3-32	193	0.013094	0.000487	0.282826	0.000012	6.1	596	844	−0.99
YHD-3-33	190	0.023093	0.000805	0.282840	0.000013	6.5	582	818	−0.98
YHD-3-34	181	0.022831	0.000798	0.282786	0.000016	4.4	656	943	−0.98
YHD-3-36	190	0.017154	0.000639	0.282790	0.000012	4.7	648	928	−0.98
YHD-3-38	192	0.027512	0.000986	0.282833	0.000012	6.3	593	832	−0.97

5. Discussion

5.1. Zircon Genesis

Zircon is a highly stable mineral [40] and can retain its primary physical and chemical properties in various geological processes. Therefore, the age and genetic information of the original rock can still be obtained by using the zircons in the altered rocks as long as the alteration does not destroy the structure and composition of the magmatic zircons.

In this paper (Sections 4.1 and 4.2), the CL image features and Th/U value of zircons from the Yanghuidongzi copper deposit show that the zircons were mainly derived from magma. In addition, since zircon is an important host mineral of U, Th, and REE in rocks [41–43], the content characteristics of these elements are also used to determine the zircon's genesis. The comparisons of the trace element characteristics of typical magmatic zircons and hydrothermal zircons by different researchers show some common features [38,44,45]. The REE patterns of magmatic zircons are generally characterized by a lower concentration of REE, with a steeper LREE (i.e., higher $(Sm/La)_N$) and higher Ce anomalies than hydrothermal zircons. The concentration of Th and U in magmatic zircons is commonly lower than that in hydrothermal zircons.

Here, we compare the REE patterns of zircons from the Yanghuidongzi copper deposit with those of the Xianshuiquan zircons [38] (Figure 5b). The REE content of the zircons in Yanghuidongzi is consistent with that of the magmatic zircons in Xianshuiquan magma and significantly lower than that of the hydrothermal zircons in Xianshuiquan. Most zircons in Yanghuidongzi have steeper LREE and higher positive Ce anomalies than hydrothermal zircons in Xianshuiquan. However, a small number of zircons in Yanghuidongzi have gentle LREE and weakly positive Ce anomalies, which indicates that some zircons may experience weak hydrothermal action.

We also compare the Th and U contents of the zircons in Yanghuidongzi with the Th and U contents of the typical magmatic zircon and hydrothermal zircon in the Bobby Plain [44] and Xianshuiquan [38]. The results show that the Th and U contents of the zircons in Yanghuidongzi are similar to those of the magmatic zircons and distinct from those of the hydrothermal zircons (Figure 6).

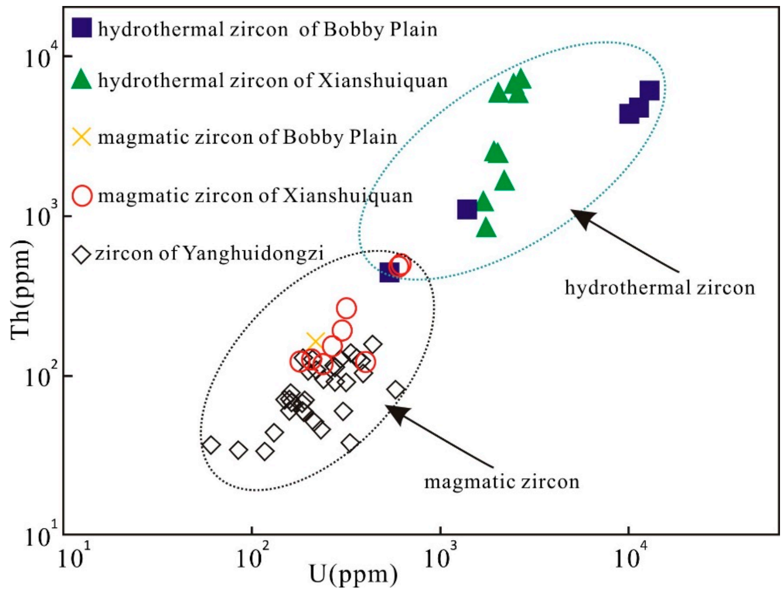

Figure 6. Th-U element covariation diagram of the Yanghuidongzi zircons.

Combined with above analysis, the zircons in Yanghuidongzi are of magmatic origin. Therefore, the zircon U-Pb ages in this paper have been affected little by later alterations and could represent the formation age of the porphyry before mineralization.

5.2. Metallogenic Age and Dynamics Background

NE China is characterized by voluminous Mesozoic granitoids, with a main diagenetic age of 160–190 Ma [14,23], forming a N–S granite belt in the eastern part of NE China (Figure 7a). Importantly, a series of Early–Middle Jurassic porphyry deposits were formed in the granite belt, consisting of an N–S porphyry copper-molybdenum metallogenic belt (Figure 7a). Combined with the chronological results in this paper, the Yanghuidongzi copper deposits (189.6 ± 1.0 Ma) are closely related to the granodiorite porphyry, which is consistent with the large-scale granite diagenetic and metallogenic ages in the area. Furthermore, the characteristics of fluid inclusion and H–O isotopes in the ore-bearing quartz veins proved that the ore-forming fluids of the Yanghuidongzi copper deposits were mainly derived from magma [22]. Therefore, the zircon U-Pb age of the granodiorite porphyry can represent both the age of the porphyry intrusion and the upper age of the magma–hydrothermal system. We hypothesized that the Yanghuidongzi porphyry copper deposit formed during the Early Jurassic (189.6 ± 1.0 Ma) and coincided with the magmatic activity in the Early Yanshanian.

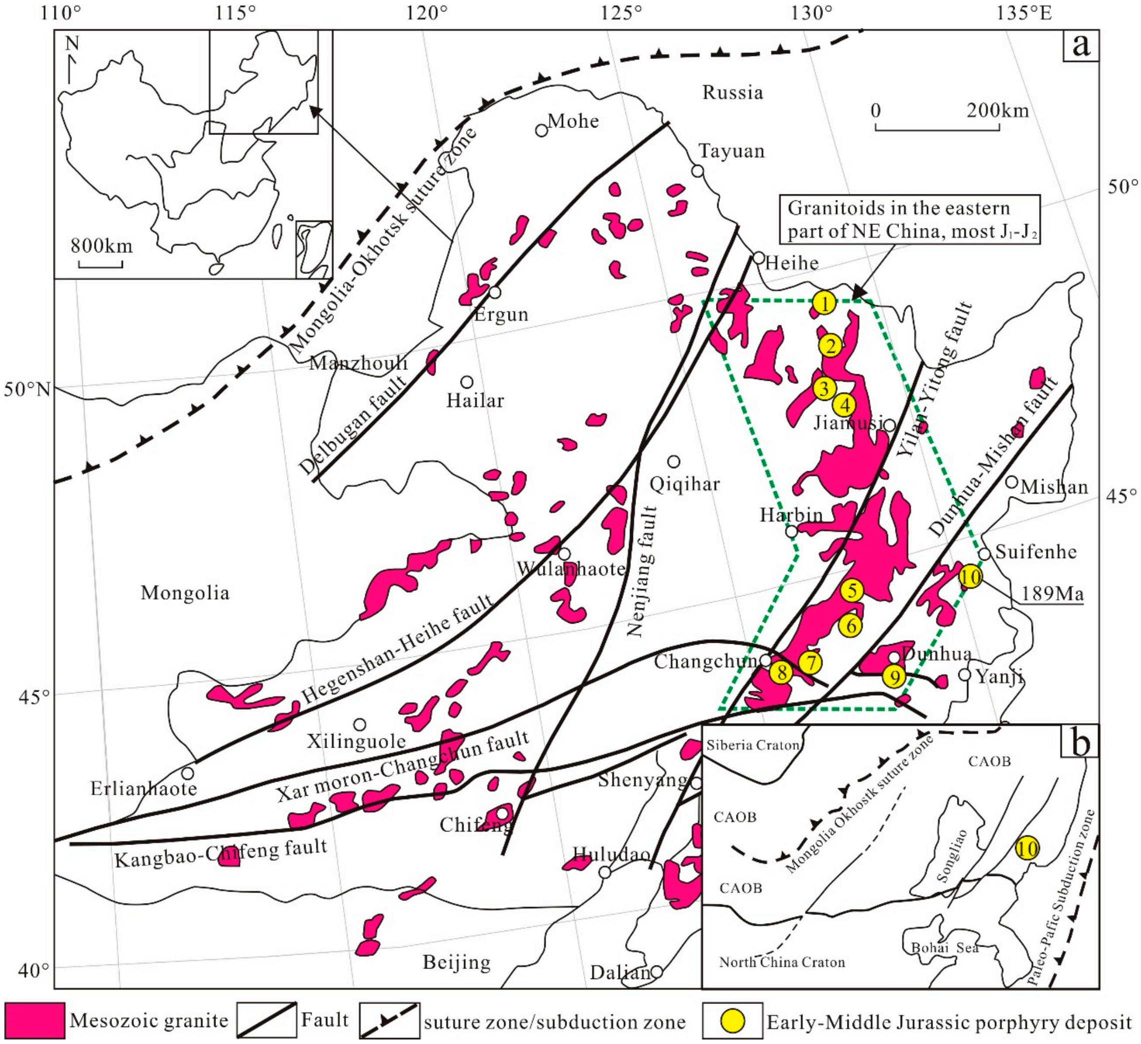

Figure 7. (**a**) Distribution of Mesozoic granites and Early–Middle Jurassic porphyry deposits in NE China [46], (**b**) the position of the Mongolia–Okhotsk suture zone and Paleo-Pacific Subduction zone relative to the study area [47,48]. 1—CuiHongshan, 2—Huojihe, 3—Cuiling, 4—Luming, 5—Fu'anbao, 6—Jidetun, 7—Daheishan, 8—Lanjia, 9—Liujiadian, 10—Yanghuidongzi. The CAOB is the Central Asian Orogenic Belt.

The geochemical elements of the porphyry rocks from the Yanghuidongzi copper deposits indicate that the mineralized granites are peraluminous calc-alkaline series I-type granitoids, characterized by an enrichment of large ion lithophile elements (LILE) and a depletion of high field strength elements (HFSE), which have similar geochemical characteristics to the subduction zone magma [21]. Furthermore, the trace elements Rb vs. (Y + Nb) and Nb vs. Y in the deposits show that the porphyry rocks were derived from volcanic arc and collisional granite, which indicates that the Yanghuidongzi copper deposit is likely to be an interaction product of plate subduction and magmatism during geological evolution [21].

The final closure of the Paleo-Asian Ocean took place during the Late Permian–Early Triassic [49,50]. After the closure of the Paleo-Asian Ocean in NE China, NE China entered the evolutionary stage of the circum-Pacific tectonic regime and the Mongolia–Okhotsk tectonic regime [51]. In the Early Jurassic, NE China experienced two subduction events: The Paleo-Pacific Plate subduction [46] and the

Mongol–Okhotsk Plate subduction [52,53]. According to the temporal and spatial distribution of the Mesozoic volcanic rocks in the Northeast, Xu et al. [46] reported that the influence of the spatial extent of the Pacific Rim tectonic system was mainly in the Songliao Basin and to its east; the influencing scope of the Mongolia-Okhotsk tectonic system was to west of the Songliao basin and the northern margin of the North China Craton. However, the Yanghuidongzi deposit is located to the east of the Songliao Basin, next to the Paleo-Pacific subduction zone, and far from the Mongolian-Okhotsk suture zone (Figure 7b). Hence, the Yanghuidongzi deposit is mostly related to the magmatism caused by the subduction of the Paleo-Pacific plate. Therefore, we can infer that the N–S Early-Middle Jurassic granite belt and porphyry deposits (including the Yanghuidongzi deposit) with similar directions to the subduction zone were formed in the eastern part of NE China during the subduction of the Paleo-Pacific plate to the East Asian continent.

5.3. Magma Source of the Ore-Bearing Porphyry

The consistency of the geochemical behavior of Nb-Ta and Zr-Hf and the ratios of Nb/Ta and Zr/Hf generally do not change in different geological processes, so their ratios can be used as powerful discriminants between different sources [54]. The Yanghuidongzi porphyry has Zr/Hf (35.48–40.0, average 38.38) and Nb/Ta (7.5–13.6, average 10.27) ratios [21] that are closer to the continental crustal values (13.4 and 36.0, respectively [55]), rather than the chondritic values (34.3 ± 0.3 and 19.9 ± 0.6, respectively [56]). This indicates that the primary magma that formed the Yanghuidongzi porphyry was generated by the partial melting of the crust material.

The Yanghuidongzi porphyry have a positive $\varepsilon_{Hf}(t)$ value (4.4–7.0) and a large $^{176}Hf/^{177}Hf$ ratio (0.282786–0.282854), with two-stage Hf model ages (T_{DM2}) ranging from 783 Ma to 943 Ma. The $\varepsilon_{Hf}(t)$ and T_{DM2} values are relatively concentrated, reflecting the isotopic uniformity of the magma source in this mining area. In addition, in the Hf isotope evolution diagram (Figure 8a,b), all points are below the line of the depleted mantle and within the ε_{Hf}(t) distribution region of the Phanerozoic igneous rocks in the eastern XMOB (Figure 8a). Most of Phanerozoic igneous rocks in the eastern XMOB have positive $\varepsilon_{Nd}(t)$ values [57,58] and positive $\varepsilon_{Hf}(t)$ values [59,60] with a younger (Nd and Hf) model age (generally 0.5–1.0 Ga), indicating that these igneous rocks were probably formed by the partial melting of Precambrian crustal material [58], and the eastern XMOB may have undergone large-scale crustal growth from the Neoproterozoic to the Phanerozoic [60].

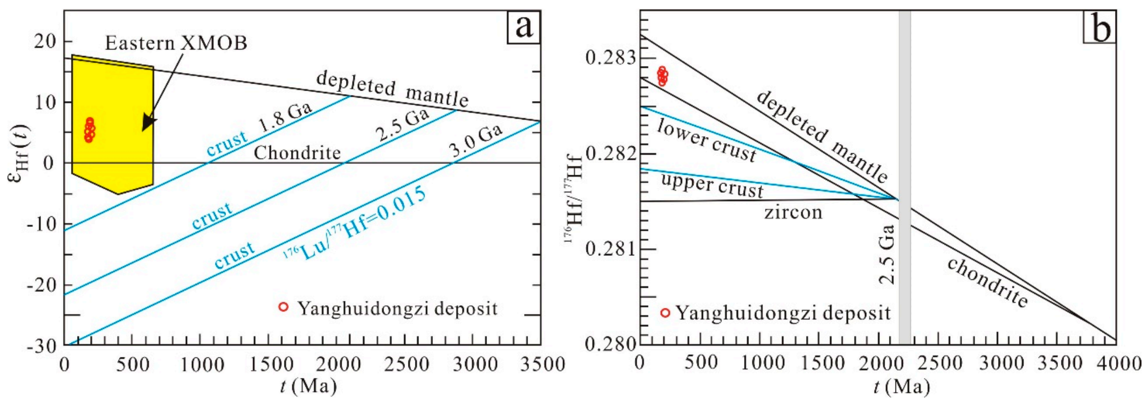

Figure 8. (**a**) Diagram of $\varepsilon_{Hf}(t)$ vs. U-Pb ages and (**b**) the $^{176}Hf/^{177}Hf$ vs. U-Pb ages of the Yanghuidongzi porphyry zircons (Hf isotopic composition of the Phanerozoic igneous rocks in the Eastern XMOB is from Yang et al. [59]).

The above analysis reveals that the primary magma that formed the Early Jurassic granodiorite porphyry in the mining area was generated by the partial melting of juvenile crustal material from the depleted mantle in the Neoproterozoic.

6. Conclusion

The combination of the zircon U-Pb and Hf isotopes of ore-bearing granodiorite porphyry from the Yanghuidongzi copper deposits provides an effective way to determine the ore-forming age, metallogenic dynamic background, and magma source.

(1) The zircon U-Pb age of the ore-bearing granite porphyry indicates that the Yanghuidongzi porphyry copper deposit was formed in the Early Jurassic (189.6 ± 1.0 Ma) and corresponds to the magmatic activity time in the area.

(2) The background analysis of ore-forming dynamics suggests that the formation of the Yanghuidongzi copper deposit was related to the subduction of the Paleo-Pacific plate.

(3) The Yanghuidongzi ore-bearing porphyry zircons have a positive $\varepsilon_{Hf}(t)$ value (4.4–7.0) and a large $^{176}Hf/^{177}Hf$ ratio (0.282786–0.282854), with the two-stage Hf model age ranging from 783 Ma to 943 Ma, which indicates that the Early Jurassic granodiorite porphyry in the mining area was formed by partial melting of the newly grown crustal material from the depleted mantle during the Neoproterozoic.

Author Contributions: Sample collection and article writing, D.C.; English writing, H.P.; Figures drawing, D.C. and H.P.; Discussion, D.C. and Y.T.; Research method, D.C., Y.T. and G.H.; Experimental design, H.P. and S.W.; Experimental data analysis, H.Y.

Funding: This research was funded by the Natural Science Foundation of Qinghai Provincial Department of Science and Technology (Grant No. 2019-ZJ-955Q), Certificate of China Postdoctoral Science Foundation (Grant No. 2019M653899XB), 2019 Qinghai University two-level financial construction special project-geological resources and geological engineering key discipline construction project (Grant No. 41250103), and Natural Science Foundation of Qinghai Provincial Department of Science and Technology (Grant No. 2017-ZJ-955Q).

Acknowledgments: The authors would like to thank the editors and the anonymous reviewers for their helpful and constructive comments.

Conflicts of Interest: The authors declare no conflict of interest.

References

1. Sillitoe, R.H. *Gold-Rich Porphyry Copper Deposits: Geological Model and Exploration Implications*; Geological Association of Canada: St.John's, NL, Canada, 1993; Volume 40, pp. 465–478.
2. Sillitoe, R.H. Characteristics and controls of the largest porphyry copper-gold and epithermal gold deposits in the circum-Pacific region. *Aust. J. Earth Sci.* **1997**, *44*, 373–389. [CrossRef]
3. Sillitoe, R.H. Porphyry copper systems. *Econ. Geol.* **2010**, *105*, 3–41. [CrossRef]
4. Richards, J.P.; Boyce, A.J.; Pringle, M.S. Geologic evolution of the escondida area, Northern Chile: A model for spatial and temporal localization of porphyry Cu mineralization. *Econ. Geol.* **2001**, *96*, 271–305. [CrossRef]
5. Kerrich, R.; Goldfarb, R.; Groves, D.; Garwin, S.; Jia, Y.F. The characteristics, origins and geodynamic setting of supergiant gold metallogenic provinces. *Sci. China* **2012**, *43*, 1–68. [CrossRef]
6. Kay, S.M.; Mpodozis, C.; Coira, B. Neogene magmatism, tectonism, and mineral deposits of the central Andes (22° to 33° S Latitude). *Soc. Econ. Geol. Spec. Publ.* **1999**, *7*, 27–59.
7. Cooke, D.R.; Wilson, A.J.; Davies, A.G.S. *Characteristics and Genesis of Porphyry Copper-Gold Deposits*; Centre for Ore Deposit Research Special Publication 5: Hobart, Tasmania, Australia, 2004; pp. 17–34.
8. Cooke, D.R.; Hollings, P.; Walshe, J.L. Giant porphyry deposits: Characteristics, distribution, and tectonic controls. *Econ. Geol.* **2005**, *100*, 801–819. [CrossRef]
9. Hou, Z.Q.; Ma, H.W.; Zaw, K.; Zhang, Y.Q.; Wang, M.J.; Wang, Z.; Pan, G.T.; Tang, R.L. The Himalayan Yulong porphyry copper belt: Product of large-scale strike-slip faulting in eastern Tibet. *Econ. Geol.* **2003**, *98*, 125–145. [CrossRef]
10. Hou, Z.Q.; Gao, Y.F.; Qu, X.M.; Rui, Z.Y.; Mo, X.X. Origin of adakitic intrusives generated during Mid-Miocene east-west extension in southern Tibet. *Earth Planet. Sci. Lett.* **2004**, *220*, 139–155. [CrossRef]
11. Hou, Z.Q.; Qu, X.M.; Rui, Z.Y.; Meng, X.J.; Li, Z.Q.; Beaudoin, G.; Rui, Z.Y.; Gao, Y.F.; Zaw, K. The Miocene gangdese porphyry copper belt generated during post-collisional extension in the Tibetan orogen. *Ore Geol. Rev.* **2009**, *36*, 25–51. [CrossRef]

12. Hou, Z.Q.; Zhang, H.R.; Pan, X.F.; Yang, Z.M. Porphyry Cu (–Mo–Au) deposits related to melting of thickened mafic lower crust: Examples from the eastern Tethyan metallogenic domain. *Ore Geol. Rev.* **2011**, *39*, 21–45. [CrossRef]
13. Qin, K.Z.; Tosdal, R.M.; Li, G.M.; Zhang, Q.; Li, J.L. Formation of the Miocene porphyry Cu (–Mo–Au) deposits in the Gangdese arc, southern Tibet, in a transitional tectonic setting. In *Mineral Deposit Research: Meeting the Global Challenge*; Zhao, C.C., Guo, B.J., Eds.; China land publishing House Place: Beijing, China, 2005; Volume 3, pp. 44–47.
14. Ge, W.C.; Wu, F.Y.; Zhou, C.Y.; Zhang, J.H. Porphyry Cu-Mo deposits in the eastern Xing'an-Mongolian Orogenic Belt: Mineralization ages and their geodynamic implications. *Chin. Sci. Bull.* **2007**, *52*, 3416–3427. [CrossRef]
15. Lee, J.; Williams, I.; Ellis, D. Pb, U and Th diffusion in nature zircon. *Nature* **1997**, *390*, 159–162. [CrossRef]
16. Cherniak, D.J.; Watson, E.B. Pb diffusion in zircon. *Chem. Geol.* **2000**, *172*, 5–24. [CrossRef]
17. Wu, Y.B.; Zheng, Y.F. Genesis of zircon and its constraints on interpretation of U-Pb age. *Chin. Sci. Bull.* **2004**, *49*, 1554–1569. [CrossRef]
18. Patchett, P.J. Importance of the Lu-Hf isotopic system in studies of planetary chronology and chemical evolution. *Geochim. Cosmochim. Acta* **1983**, *47*, 81–91. [CrossRef]
19. Wang, F.; Zhu, L.; Li, J.; Lee, B.; Gong, H.; Yang, T.; Wang, W.; Xu, A. Zircon U-Pb ages and Hf isotopic characteristics of the Dehe biotite monzonitic gneiss pluton in the North Qinling orogen and their geological significance. *Chin. J. Geochim.* **2011**, *30*, 204–216. [CrossRef]
20. Wu, F.Y.; Li, X.H.; Zheng, Y.F.; Gao, S. Lu-Hf isotopic systematics and their application in petrology. *Acta Petrol. Sin.* **2007**, *23*, 185–220. (In Chinese)
21. Lv, J.C. The Ore-Forming Geological Conditions and Prospecting Orientation of Yanghuidongzi Cu Deposit. Master's Thesis, Jilin University, Changchun, China, 2014. (In Chinese).
22. Zhu, J.Q.; Sun, J.G.; Men, L.J.; Gu, A.L.; Chen, Y.J.; Ming, Z.; Zhao, S.F.; Yan, J. Metallogenic mechanism of Yanghuidongzi copper deposit in eastern Heilongjiang Province: Mineralization-alteration, fluid inclusions and stable isotope tracing. *Depos. Geol.* **2016**, *35*, 365–380. (In Chinese)
23. Wu, F.Y.; Sun, D.Y.; Ge, W.C.; Zhang, Y.B.; Grant, M.L.; Wilde, S.A.; Jahn, B.M. Geochronology of the Phanerozoic granitoids in northeastern China. *J. Asian Earth Sci.* **2011**, *41*, 1–31. [CrossRef]
24. Zhang, B.C. *Detailed Report on Yanghuidong Copper Mine in Dongning County*; Heilongjiang Province Nonferrous Metals Geological Exploration 702 Team: Mudanjiang, China, 2009. (In Chinese)
25. Zhao, S.; Xu, D.H.; Wang, Y.P. *Regional Geological Survey Report of the People's Republic of China 1:50,000 (L52E022020 Suiyang Town)*; Heilongjiang Provincial Geological Survey and Research Institute: Harbin, China, 2011. (In Chinese)
26. Eggins, S.M.; Kinsley, L.P.J.; Shelley, J.M.G. Deposition and element fractionation processes during atmospheric pressure laser sampling for analysis by ICP-MS. *Appl. Surf. Sci.* **1998**, *127–129*, 278–287. [CrossRef]
27. Jackson, S.E.; Pearson, N.J.; Griffin, W.L.; Belousova, E.A. The application of laser ablation-inductively coupled plasma-mass spectrometry to in situ U–Pb zircon geochronology. *Chem. Geol.* **2004**, *211*, 47–70. [CrossRef]
28. Wiedenbeck, M. An example of reverse discordance during ion microprobe zircon dating: An artifact of enhanced ion yields from a radiogenic labile Pb. *Chem. Geol.* **1995**, *125*, 197–219. [CrossRef]
29. Yuan, H.; Gao, S.; Liu, X.M.; Li, H.M.; Gunther, D.; Wu, F.Y. Accurate U-Pb age and trace element determinations of zircon by laser ablation-inductively coupled plasma-mass spectrometry. *Geostand. Geoanal. Res.* **2004**, *28*, 353–371. [CrossRef]
30. Ludwig, K.R. *Isoplot 3.0: A Geochronological Toolkit for Microsoft Excel*; Berkeley Geochronology Center: Berkeley, CA, USA, 2003; p. 70.
31. Wiedenbeck, M.; Alle, P.; Corfu, F.; Griffin, W.L.; Meier, M.; Oberli, F.; Quadt, A.V.; Roddick, J.C.; Spiegel, W. Three natural zircon standards for U-Th-Pb, Lu-Hf, trace element and REE analyses. *Geostandard. Newslett.* **1995**, *19*, 1–23. [CrossRef]
32. Wu, F.Y.; Yang, Y.H.; Xie, L.W.; Yang, J.H.; Xu, P. Hf isotopic compositions of the standard zircons and baddeleyites used in U-Pb geochronology. *Chem. Geol.* **2006**, *234*, 105–126. [CrossRef]

33. Woodhead, J.; Hergt, J.; Shelley, M.; Eggins, S.; Kemp, R. Zircon Hf-isotope analysis with an excimer laser, depth profiling, ablation of complex geometries, and concomitant age estimation. *Chem. Geol.* **2004**, *209*, 121–135. [CrossRef]
34. Blicherttoft, J.; Albarède, F. The Lu-Hf isotope geochemistry of chondrites and the evolution of the mantle-crust system. *Earth Planet. Sci. Lett.* **1998**, *154*, 243–258. [CrossRef]
35. Griffin, W.L.; Pearso, N.J.; Belousova, E.; Jackson, S.E.; Achterbergh, E.; O'Reilly, S.Y.; Shee, S.R. The Hf isotope composition of cratonic mantle: LAM-MC-ICPMS analysis of zircon megacrysts in kimberlites. *Geochim. Cosmochim. Acta* **2000**, *64*, 133–147. [CrossRef]
36. Griffin, W.L.; Wang, X.; Jackson, S.E.; Pearson, N.J.; O'Reilly, S.Y.; Xu, X.S.; Zhou, X.M. Zircon chemistry and magma mixing, SE China: In-situ analysis of Hf isotopes, Tonglu and Pingtan igneous complexes. *Lithos* **2002**, *61*, 237–269. [CrossRef]
37. Corfu, F.; Hanchar, J.M.; Hoskin, P.W.O.; Kinny, P. Atlas of zircon textures. *Rev. Mineral. Geochem.* **2003**, *53*, 469–500. [CrossRef]
38. Tang, J.H.; Gu, L.X.; Zhang, Z.Z.; Wu, C.Z.; San, J.Z.; Wang, C.S.; Liu, S.H.; Zhang, G.H. Hyperplastic edge CL of hydrothermal and character- istics of REE for zircon of Xianshuiquan gneissic granite Hyperplastic edge CL of hydrothermal and character- istics of REE for zircon of Xianshuiquan gneissic granite. *Prog. Nat. Sci.* **2008**, *18*, 769–777. (In Chinese)
39. McDonough, W.F.; Sun, S.-S. The composition of the Earth. *Chem. Geol.* **1995**, *120*, 223–253. [CrossRef]
40. Curtis, C.E.; Sowman, H.G. Investigation of the Thermal Dissociation, Reassociation, and Synthesis of Zircon. *J. Am. Ceram. Soc.* **1953**, *36*, 190–198. [CrossRef]
41. Sawka, W.N. REE and trace element variations in accessory minerals and hornblende from the strongly zoned McMurry Meadows Pluton, California. *Earth Sci.* **1988**, *79*, 157–168. [CrossRef]
42. Bea, F. Residence of REE, Y, Th and U in granites and crustal protoliths, implications for the chemistry of crustal melts. *J. Petrol.* **1996**, *97*, 521–552. [CrossRef]
43. O'Hara, M.J.; Fry, N.; Prichard, H.M. Minor phase as carriers of trace elements in non-modal crystal-liquid separation processes I: Basic relationships. *J. Petrol.* **2001**, *42*, 1869–1885. [CrossRef]
44. Hoskin, P.W.O. Trace-element composition of hydrothermal zircon and the alteration of Hadean zircon from the Jack Hills, Australia. *Geochim. Cosmochim. Acta* **2005**, *69*, 637–648. [CrossRef]
45. Fu, B.; Mernagh, T.P.; Kita, N.T.; Kemp, A.I.S.; Valley, J.W. Distinguishing magmatic zircon from hydrothermal zircon: A case study from the Gidginbung high-sulphidation Au–Ag–(Cu) deposit, SE Australia. *Chem. Geol.* **2009**, *259*, 131–142. [CrossRef]
46. Xu, W.L.; Wang, F.; Pei, F.P.; Meng, E.; Tang, J.; Xu, M.J.; Wang, W. Mesozoic tectonic regimes and regional ore-forming background in NE China: Constraints from spatial and temporal variations of Mesozoic volcanic rock associations. *Acta Petrol. Sin.* **2013**, *29*, 339–353. (In Chinese)
47. Wang, T.; Zheng, Y.D.; Zhang, J.J.; Zeng, L.S.; Donskaya, T.V.; Guo, L.; Li, J.B. Pattern and kinematic polarity of late Mesozoic extension in continental NE Asia: Perspectives from metamorphic core complexes. *Tectonics* **2011**, *30*, TC6007. [CrossRef]
48. Wang, T.; Guo, L.; Zheng, Y.D.; Donskaya, T.; Gladkochub, D.; Zeng, L.S.; Li, J.B.; Wang, Y.B.; Mazukabov, A. Timing and processes of late Mesozoic mid-lower-crustal extension in continental NE Asia and implications for the tectonic setting of the destruction of the North China Craton: Mainly constrained by zircon U–Pb ages from metamorphic core complexes. *Lithos* **2012**, *154*, 315–345. [CrossRef]
49. Li, J.Y. Permian geodynamic setting of Northeast China and adjacent regions: Closure of the Paleo-Asian Ocean and subduction of the Paleo-Pacific Plate. *J. Asian Earth Sci.* **2006**, *26*, 207–224. [CrossRef]
50. Xiao, W.J.; Windley, B.F.; Huang, B.C.; Han, C.M.; Yuan, C.; Chen, H.L.; Sun, M.; Sun, S.; Li, J.L. End Permian to mid-Triassic termination of the southern Central Asian Orogenic Belt. *Int. J. Earth Sci.* **2009**, *98*, 1189–1217. [CrossRef]
51. Cao, H.H.; Xu, W.L.; Pei, F.P.; Wang, Z.W.; Wang, F.; Wang, Z.J. Zircon U-Pb geochronology and petrogenesis of the Late Paleozoic-Early Mesozoic intrusive rocks in the eastern segment of the northern margin of the North China Block. *Lithos* **2013**, *170–171*, 191–207. [CrossRef]
52. Xu, W.L.; Pei, F.P.; Wang, F.; Meng, E.; Ji, W.Q.; Yang, D.B.; Wang, W. Spatial–temporal relationships of Mesozoic volcanic rocks in NE China: Constraints on tectonic overprinting and transformations between multiple tectonic regimes. *J. Asian Earth Sci.* **2013**, *74*, 167–193. [CrossRef]

53. Zhang, J.H.; Ge, W.C.; Wu, F.Y.; Wilde, S.A.; Yang, J.H.; Liu, X.M. Large-scale Early Cretaceous volcanic events in the northern Great Xing'an Range, northeastern China. *Lithos* **2008**, *102*, 138–157. [CrossRef]
54. Hoffmann, J.E.; Münker, C.; NaRaa, T.; Rossing, M.T.; Herwartz, D.H.; Schönberg, D.G.; Svahnberg, H. Mechanisms of Archean crust formation inferred from high-precision HFSE systematics in TTGs. *Geochim. Cosmochim. Acta* **2011**, *75*, 4157–4178. [CrossRef]
55. Rundnick, R.L.; Gao, S. Composition of the continental crust. In *Treatise on Geochemistry*; Holland, H.D., Turekian, K., Eds.; Elsevier: Amsterdam, The Netherlands, 2004; Volume 3, pp. 1–64.
56. Munker, C. Evolution of Planetary Cores and the Earth-Moon System from Nb/Ta Systematics. *Science* **2003**, *301*, 84–87. [CrossRef]
57. Jahn, B.M.; Wu, F.Y.; Chen, B. Granitoids of the Central Asian Orogenic Belt and continental growth in the Phanerozoic. *R. Soc. Edinb.* **2000**, *91*, 181–193. [CrossRef]
58. Wu, F.Y.; Jahn, B.M.; Wilde, S.; Sun, D.Y. Phanerozoic crustal growth: U-Pb and Sr-Nd isotopic evidence from the granite in northeastern China. *Tectonophysics* **2000**, *328*, 89–113. [CrossRef]
59. Yang, J.H.; Wu, F.Y.; Shao, J.A.; Wilde, S.A.; Xie, L.W.; Liu, X.M. Constraints on the timing of uplift of the Yanshan Fold and Thrust Belt, North China. *Earth Planet. Sci. Lett.* **2006**, *246*, 336–352. [CrossRef]
60. Ji, Z.; Ge, W.C.; Wang, Q.H.; Hao, Y.; Guo, C.Z.; Jun, H.B.; Yu, D. Petrogenesis of Early Cretaceous volcanic rocks of the Manketouebo Formation in the Wuchagou region, central Great Xing'an Range, NE China, and tectonic implications: Geochronological, geochemical, and Hf isotopic evidence. *Int. Geol. Rev.* **2015**, *58*, 556–573. [CrossRef]